analytical chemistry

Article

Cite This: *Anal. Chem.* 2019, 91, 2169−2176

pubs.acs.org/ac

SwissKnife-Inspired Multifunctional Fluorescence Probes for Cellular Organelle Targeting Based on Simple AIEgens

Jen-Shyang Ni,[†,‡] Michelle M. S. Lee,[†,‡,§] Pengfei Zhang,[‡,§,∥] Chen Gui,[‡,§] Yuncong Chen,[‡,§] Dong Wang,[‡,⊥] Zhen-Qiang Yu,[⊥] Ryan T. K. Kwok,[‡,§] Jacky W. Y. Lam,[‡,§] and Ben Zhong Tang*[,‡,§,#]

[‡]HKUST-Shenzhen Research Institute, No. 9 Yuexing first RD, South Area, Hi-tech Park, Shenzhen 518057, China

[§]Department of Chemistry, Hong Kong Branch of Chinese National Engineering Research Center for Tissue Restoration and Reconstruction, Institute for Advanced Study and Division of Life Science, Hong Kong University of Science and Technology, Clear Water Bay, Kowloon, Hong Kong

[∥]Guangdong Key Laboratory of Nanomedicine, Shenzhen engineering Laboratory of nanomedicine and nanoformulations, CAS Key Laboratory of Health Informatics, Institute of Biomedicine and Biotechnology, Shenzhen Institutes of Advanced Technology, Chinese Academy of Sciences, Shenzhen 518055, China

[⊥]Center for AIE Research, College of Materials Science and Engineering, Department of Chemistry and Environmental Engineering, Shenzhen University, Shenzhen 518060, China

[#]SCUT-HKUST Joint Research Laboratory, State Key Laboratory of Luminescent Materials and Devices, South China University of Technology, Guangzhou 510640, China

Supporting Information

ABSTRACT: Facile, efficient, and mass production of aggregation-induced emission (AIE) luminogens (AIEgens) with excited-state intramolecular proton transfer (ESIPT) characteristics was achieved by a one-step condensation reaction of 2-(hydrazonomethyl)phenol with benzaldehydes. The function of as-prepared AIEgens could be tuned easily by varying the functional group being carried on the phenyl ring of benzaldehyde just like a Swiss knife handle. The suitable distance and angle of the intramolecular hydrogen bond in these AIEgens endowed them with ESIPT properties, intense solid-state luminescence, and large Stokes shifts (155−169 nm). These AIEgens could not only serve as biological probes showing specific targeting to lipid droplets, endoplasmic reticulum, and lysosomes, respectively, but also generate reactive oxygen species upon visible light irradiation to make them promise for photodynamic therapy.

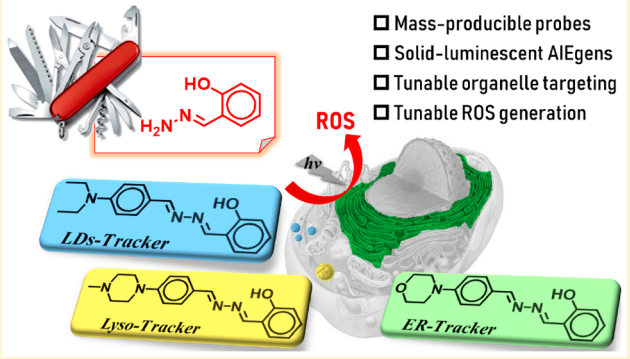

As the essential part, cellular organelles are vital for the cell to live. Each organelle plays an important role to support the normal functions of cells and the life of the whole body. For instance, the lipid droplets (LDs), as the place of energy storage for neutral lipid, involve some significantly important biofunctions,[1] such as dynamic regulations of the storage and metabolism of neutral lipids, membrane maintenance, and protein trafficking, maturation, and degradation.[2] Lysosome, a monolayered digestive compartment in the cell with a low pH (ca. 4.50),[3] is primarily responsible for degrading biomacromolecules into low-molecular-weight materials and is also involved in numerous key life activities including intracellular transportation, apoptosis, cholesterol homeostasis, and plasma membrane repair.[4−6] As a crucial organelle around eukaryotic cell's nucleus, endoplasmic reticulum (ER) covered over half of the total membranes of a cell and can be divided into rough ER and smooth ER according to the composition of its phospholipid membrane. The former is coated with ribosomes for the production of functional three-dimensional proteins, and the latter in regions without ribosomes mainly acts as a signaling station, including calcium, nucleotides, various enzymes, sterols, and reactive oxygen species (ROS).[7,8] Besides, ER is also fundamental to the regulation of calcium homeostasis and synthesis of proteins, lipids and carbohydrates. It has demonstrated that organelle dysfunction would cause a series of diseases, such as cancer, Parkinson's disease,[9] Alzheimer's disease,[10−12] and diabetes.[13] Thus, specific organelle-targeting can not only be able to track their morphological changes to aid the understanding of their

Received: October 15, 2018
Accepted: December 28, 2018
Published: December 28, 2018

DOI: 10.1021/acs.analchem.8b04736
Anal. Chem. 2019, 91, 2169−2176

biological roles, but also as potential therapeutic targets for the prediction and treatment of a variety of diseases.[14,15]

Biological fluorometric detection has been paid attention in the field of bioimaging technology with the progress of human civilization. Due to the expensive purification and tedious transfected processes of fluorescent proteins, commercial organelle-targeting based on small organic or organometallic molecules have been broadly used for colocalization assays. Among them, metal-free organic probes such as BODIPY and Nile red (Scheme S1) have been more popular with scientists by reason for their low cytotoxicity and low cost.[16] However, such traditional commercial probes suffer from aggregation-caused quenching phenomenon, implying fluorescent self-quenching in high concentration or solid/aggregated states, which remains the major barrier to their practical applications. By contrast, aggregation-induced emission (AIE) luminogens (AIEgens),[17−20] with no or dim emission in the disperse state, but high in the solid or aggregated states, have acted as the promise candidate for organelle-targeting probes to study the functions of organelles in terms of more advantages of high photostability, good biocompatibility, turn-on feature in favor of contrast-enhancing and wash-free preparation, and large Stokes shift avoiding the interference from background fluorescence and the excitation source.[15,21−23] Thus, the development of functional and specially targeting AIEgens is an important aspect of fluorescent detection technology.

More and more AIE mechanisms being proposed, such as restriction of intramolecular motions (RIM),[24,25] twisted intramolecular change transfer (TICT),[26−28] excited-state double-bond reorganization (ESDBR),[29] and excited-state intramolecular proton transfer (ESIPT),[30−33] assisted us for fully understanding the luminous principle of AIEgens as well as constructing novel structures. It is well-known that, compared to common fluorophores, ESIPT-active chromophores usually have multiple and tunable emissions and exhibit remarkably large Stokes shifts (>150 nm)[34] without self-absorption as a result of their unique photoinduced photophysical process of enol−keto tautomerization through pre-existing intramolecular hydrogen-bond (H-bond) in the excited state.[22,35,36] In the solid or aggregation states, the ratio of keto-form emission will be largely enhanced promoting the growth of radiative pathway.[12,34,37] Meanwhile, due to the RIM effect, nonradiative pathways are suppressed to be conductive to solid-emission. It is worth being thought whether we can utilize an ESIPT- or an AIE-active unit to regulate the AIEgens to target the unalike organelles, like the multifunctional Swiss knife. If successful, this strategy not only supports us to understand in depth the relationship between molecular structure and organelle-localization but also puts forward the potential requirements of commercialization, low-cost and high efficiency.[38]

To achieve this organelle-targeting regulating strategy, in this investigation, we utilized an ESIPT-active unit, 2-(hydrazono-methyl)phenol (H-AP) (Scheme 1)[39] and aldehyde derivatives to construct the salicylaldehyde-based Schiff-base molecules. The H-AP unit possesses various inherent properties: (i) its amino group can be condensed with benzaldehyde derivatives facilely and efficiently, (ii) it is hydrophilic and can be adjusted to amphiphilic molecules after being tied to the lipophilic segment, (iii) it contains basic nitrogen atom and acidic hydroxy proton with close proximity which favorably forms the intramolecular H-bond in the excited state upon photo-excitation, (iv) it shows ESIPT-active to be helpful to the large

Scheme 1. Structures of ESIPT-Active AIEgens

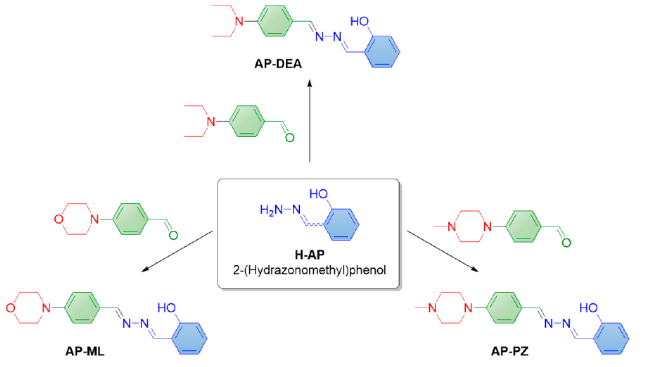

Stokes shift between absorption of enol-form and emission of keto-form, and (v) it adopts a low steric and relatively coplanar structure to favor electronic communication with the nearby groups and intramolecular proton transfer in the excited state. By introducing and regulating the different lipophilic groups including diethylamino, morpholine and 1-methylpiperazine, these corresponding ESIPT-active AIEgens, abbreviated as AP-DEA, AP-ML, and AP-PZ, were constructed by very facile synthetic procedures (Scheme 1). Served as biological fluorescent probes, they could not only specifically locate and accumulate in LDs, ER, and lysosome, respectively, with low cytotoxicity in dark but also generate ROS under illumination.

EXPERIMENTAL SECTION

Materials and Methods. 4-Diethylaminobenzaldehyde, 4-morpholinobenzaldehyde, 2′,7′-dichlorofluorescin diacetate (DCFH-DA), 4-(4-methylpiperazin-1-yl)-benzaldehyde, and other chemicals were purchased from Energy Chemical, Derthon, Meryer, Bide Pharmatech and Sigma-Aldrich and used without further purification. Solvents were directly used without further purification. ^{1}H and ^{13}C NMR spectra were recorded on the Varian VNMRS 400 using $CDCl_3$ as solvent and tetramethylsilane as internal standard. UV−vis absorption and photoluminescence (PL) spectra were recorded on a Shimadzu UV-2600 spectrometer and PerkinElmer LS 55 fluorescence spectrometer, respectively. The absolute quantum yields of the solid powder and solution were determined using a Hamamatsu C11347−11 Quantaurus-QY Analyzer. The lifetime was recorded on an Edinburgh FLS 980 instrument and measured by time-correlated single-photon counting method.

Synthetic Procedures of AP-Based Probes. 2-(Hydrazono-methyl)phenol (1 equiv) and aldehyde derivatives (1 equiv) were dissolved in ethanol (100 mM) and then stirred at room temperature overnight. The mixture was cooled to 0 °C, and the precipitate was filtered, washed with a little cool ethanol, and collected without column chromatography. After dried under vacuum, the pure product was obtained. Single crystals for single crystal X-ray diffraction analysis were gained in chloroform/hexane with slow layer-to-layer diffusion.

Characterization Data of AP-DEA: Yellow Solid, 96% Yield. ^{1}H NMR (400 MHz, $CDCl_3$), δ (ppm): 11.85 (s, 1H), 8.71 (s, 1H), 8.49 (s, 1H), 7.69 (d, 2H, J = 8.4 Hz), 7.34−7.30 (m, 2H), 7.01 (d, 1H, J = 8.4 Hz), 6.92 (t, 1H, J = 7.4 Hz), 6.69 (d, 2H, J = 8.0 Hz), 3.45−3.39 (m, 4H), 1.22−1.19 (m, 6H). ^{13}C NMR (100 MHz, $CDCl_3$), δ (ppm): 162.68, 162.45, 162.34, 162.05, 159.59, 150.31, 132.23, 132.04, 131.83, 131.62,

DOI: 10.1021/acs.analchem.8b04736
Anal. Chem. 2019, 91, 2169−2176

130.91, 130.58, 120.17, 119.35, 119.19, 118.23, 116.92, 116.67, 111.22, 111.07, 44.52, 12.69, 12.45. HRMS (MALDI-TOF): Calcd for $C_{18}H_{21}N_3O$ $[M]^+$, 295.1685; found, 295.1675.

Characterization Data of AP-ML: Yellow Solid, 93% Yield. ^{1}H NMR (400 MHz, $CDCl_3$), δ (ppm): 11.85 (s, 1H), 8.74 (s, 1H), 8.53 (s, 1H), 7.76 (d, 2H, J = 8.8 Hz), 7.36−7.32 (m, 2H), 7.02 (d, 1H, J = 8.0 Hz), 6.95−6.92 (m, 3H), 3.88−3.85 (m, 4H), 3.30−3.28 (m, 4H). ^{13}C NMR (100 MHz, $CDCl_3$), δ (ppm): 163.62, 163.32, 162.15, 161.91, 159.69, 153.38, 132.69, 132.28, 131.88, 130.46, 130.16, 124.21, 119.47, 119.30, 117.95, 117.02, 116.77, 115.16, 114.50, 114.34, 66.82, 66.60, 66.37, 47.98, 47.88. HRMS (MALDI-TOF): Calcd for $C_{18}H_{19}N_3O_2$ $[M]^+$, 309.1477; found, 309.1476.

Characterization Data of AP-PZ: Yellow Solid, 95% Yield. ^{1}H NMR (400 MHz, $CDCl_3$), δ (ppm): 11.89 (s, 1H), 8.72 (s, 1H), 8.52 (s, 1H), 7.73 (d, 2H, J = 8.8 Hz), 7.35−7.31 (m, 2H), 7.02 (d, 1H, J = 8.0 Hz), 6.94−6.92 (m, 3H), 3.38−3.35 (m, 4H), 2.59−2.56 (m, 4H), 2.36 (s, 3H). ^{13}C NMR (100 MHz, $CDCl_3$), δ (ppm): 163.41, 163.11, 162.29, 162.04, 159.68, 153.29, 132.21, 130.40, 130.09, 123.72, 119.42, 118.01, 116.99, 116.74, 115.34, 114.66, 114.50, 54.77, 47.56, 46.24, 45.94. HRMS (MALDI-TOF): Calcd for $C_{19}H_{22}N_4O$ $[M]^+$, 322.1794; found, 322.1795.

Cell Imaging and Confocal Colocalization. HeLa cells were cultured in the minimum essential medium eagle (MEM) containing 10% fetal bovine serum (FBS) and antibiotics (100 units/mL penicillin and 100 mg/mL streptomycin) in a 5% CO_2 humidity incubator at 37 °C. After HeLa cells were incubated with AP-based AIEgens (1 μM) and the commercial probes (500 nM) at 37 °C for 30 min, the medium was removed and the cells were rinsed with phosphate buffer saline (PBS) three times and then imaged under a confocal microscope (LSM710). The excitation was 405 nm for AP-based AIEgens and 560 nm for ER-Tracker Red, LysoTracker Deep Red, MitoTracker Red, and Nile red. The emission filter was 448−548 nm for AP-based AIEgens and 598−753 nm for the commercial probes.

ROS Generation Analysis. A total of 25 μL of 2′,7′-dichlorodihydrofluo-rescein (DCFH; 40 μM), hydrolyzed DCFH-DA (Scheme S3) by sodium hydroxide (NaOH), as an indicator was added into AP-based AIEgens (10 μM) of PBS solution (1 mL). After the different irradiation time of white LED, the emission signal of 2′,7′-dichlorofluorescein (DCF) was measured one by one, in which the excitation was 480 nm. The relative emission intensity (I/I_0 − 1) at 525 nm versus irradiation time was plotted. Besides, AP-based AIEgens or DCFH alone under irradiation were the control.

Cytotoxicity Study in Dark and under Light Irradiation. Cells were seeded in 96-well plates (Costar, IL, U.S.A.) at a density of 5000 cells/well. After overnight culturing, the medium in each well were replaced by 100 μL of fresh medium containing different concentrations of AIEgens. After 24 h incubation, 10 μL of MTT solution (5 mg/mL in PBS) was added into each well and incubated for 4 h. After a further 30 min of incubation under light irradiation, in which another array of plates in the dark was used as the control, 100 μL of DMSO was added to each well and then vibrated for 15 min. The absorption of each well at 595 nm was recorded via a plate reader (PerkinElmer Victor3TM). Each trial was performed with 6 wells parallel.

RESULTS AND DISCUSSION

Design and Synthesis. The synthetic protocols for AP-DEA, AP-ML, and AP-PZ are illustrated in Scheme 1, and experimental details are given in the Supporting Information (SI). The starting material, 2-(hydrazonomethyl)phenol (H-AP),[39] was synthesized from salicylaldehyde and hydrazine and used without further purification by column chromatography. After being condensed with benzaldehyde derivatives, AP-DEA, AP-ML, and AP-PZ were obtained with a yield of 93−96%. All of the materials were characterized by nuclear magnetic resonance (NMR) spectroscopy, high-resolution mass spectrometry (HRMS), and single crystal X-ray diffraction analysis. Compared to the classic organometallic probes such as iridium or ruthenium complexes, owing to high yield and facile synthesis of ESIPT-active AIEgens, these productions could be increased to the level of grams effortlessly (Figure S1) with low cost.

Optical and AIE Properties. The UV−vis absorption spectra of AP-DEA, AP-ML, and AP-PZ in tetrahydrofuran (THF) at a concentration of 10 μM were shown in Figure 1A

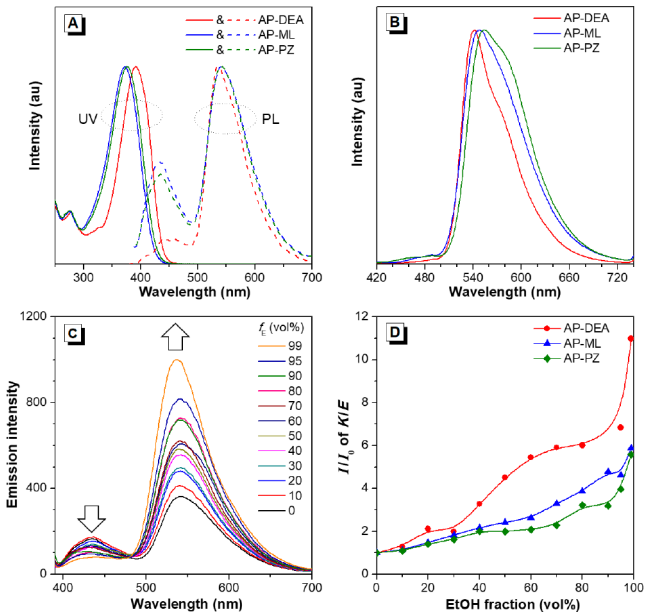

Figure 1. (A) Normalized UV−vis and photoluminescence (PL) spectra of AIEgens in THF, (B) normalized PL of AIEgens in the solid state, (C) PL spectra versus the ethanol (EtOH) faction (f_E) of the THF/EtOH mixtures (vol%) for AP-PZ, and (D) change of relative emission intensity (I/I_0) vs the f_E values for AIEgens.

and the relevant data are listed in Table 1. They had similar absorption spectra of $\pi-\pi$ and charge transfer (CT) band for enol-form,[40] which was corresponding with the trend of theoretical calculation data (Table S1). AP-DEA showed high proportion of keto-form emission as opposed to enol-form in comparison with AP-ML and AP-PZ, implying that close-heterocyclic alkyl-ring (morpholine and methyl-piperazine) limits the ESIPT effect of molecules maybe. Besides, all of these materials not only had large Stokes shift (155−169 nm) by means of ESIPT process, but also showed the typical AIE features (Figure 1D) upon the addition of a water fraction (Figure S2). However, the protic solvent (water) had some obvious interference on the intramolecular proton transfer of ESIPT-active materials.[22] To eliminate/decline the protic

DOI: 10.1021/acs.analchem.8b04736
Anal. Chem. 2019, 91, 2169−2176

Table 1. Photophysical Properties of AP-DEA, AP-ML, and AP-PZ

	THF solution[a]					solid powder		
AIEgens	λ_{abs} (nm)	λ_{em}[b] (Φ; nm, %)	τ[c] (k_r, k_{nr}; ns, ns^{-1}, ns^{-1})	Δ_{THF}[d] (nm)	E_g[e] (eV)	λ_{em} (Φ; nm, %)	τ (k_r, k_{nr}; ns, ns^{-1}, ns^{-1})	α_{AIE}[f]
AP-DEA	391	457 (0.10), 535 (1.30)	0.45 (0.03, 2.20), 0.41 (0.31, 2.43)	45, 155	2.83	542 (15.20)	1.31 (1.16, 6.47)	10.99
AP-ML	372	433 (0.10), 541 (0.30)	0.72 (0.01, 1.38), 0.54 (0.06, 1.86)	61, 169	2.92	548 (5.70)	0.94 (0.61, 9.98)	5.89
AP-PZ	376	435 (0.20), 541 (0.50)	0.59 (0.03, 1.70), 0.58 (0.09, 1.71)	59, 165	2.90	554 (8.60)	1.02 (0.85, 8.98)	5.59

[a]Recorded at 298 K (10 μM). [b]Quantum yield (Φ) measured by a calibrated integrating sphere. [c]Rate constants for radiative (k_r) and nonradiative decay (k_{nr}) calculated from Φ and lifetime (τ) values according to $k_r = \Phi/\tau$ and $k_{nr} = (1 - \Phi)/\tau$. [d]Δ_{THF} = Stokes shift = $\lambda_{em} - \lambda_{abs}$. [e]Band gap ($E_g$) calculated from the onset wavelength (λ_{onset}) of the absorption spectra, $E_g = 1240/\lambda_{onset}$. [f]$\alpha_{AIE}$ was the relative emission intensity (I/I_0) based on the ratio of keto- and enol-form in the 99 vol % ethanol fractions of the THF/ethanol mixtures.

effect of solvent and clearly study the enol−keto tautomerization of ESIPT property, herein, the weakly protic type solvent (ethanol) and tetrahydrofuran (THF) were used as poor and good solvents, respectively. Along with the increase of ethanol fraction, the emission intensity of enol-form was weakened gradually, in contrast, that of keto-form was enhanced (Figures 1C,D, S3, and S4). Due to the RIM mechanism in the aggregated state, the molecular conformation would be coplanarized to be beneficial for intramolecular hydrogen-bonding and keto-tautomer forming in the excited state upon photoexcitation. Thus, in the aggregated or solid states, keto-forming emission could be observed mainly (Figure 1B), and the heightened relative emission intensity (I/I_0) based on the ratio of keto- to enol-forms (K/E) was mainly attributed to the effect of ESIPT-active AIEgens (Figures 1C and S3).

Further to analyze the lifetime and quantum yield (QY) by using time-resolved fluorescence spectroscopy (Figure S5) and calibrated integrating sphere of absolute method, respectively, it was observed that both lifetime and QY in the solid state were promoted in comparison with those in THF solution (Table 1) as the result of the increasing radiative rate (k_r) and the decreasing nonradiative rate (k_{nr}) of keto-form. The former grew about 4−10-fold owing to more formation of the excited keto-tautomer to be helpful for emission via radiative pathway, and the latter dropped about 2−4-fold due to the RIM effect declining the energy loss of excited molecules via nonradiative pathway. Both factors positively contribute to AIE feature and solid-luminescence.

Theoretical Calculation Study. To decipher the photophysical mechanism of AIEgens in THF solution, theoretical calculations with time-dependent density functional theory (TD-DFT) at the level of B3LYP/6-31G* based on solvation of THF was used to optimize the molecular geometries in the ground (S_0) and excited (S_1) states, and their molecular frontier orbitals and detail calculation data were summarized in Figures 2, S6, and S7 and Tables S1−S5. The results of the calculations clearly showed that the quite coplanar geometries were favorable for proton transfer in the excited state, that is, the torsions were very small. Both electron densities of HOMO and LUMO were therefore distributed to the whole molecule. The variation in electron density from HOMO to LUMO of the phenolic oxygen atom decreased, and that of the nitrogen atom in the azo-group increased. This suggested that improvements in both the basicity of the nitrogen and the acidity of the phenolic hydroxyl group would facilitate ESIPT from oxygen to nitrogen. In addition, for S_1 geometries, the elongation of bonds between phenolic hydrogen and oxygen (O−H, 1.01 Å) and shortening of the distances between nitrogen and phenolic hydrogen (N···H, 1.70−1.71 Å) were observed, in which were compared to S_0 geometries (0.998 and

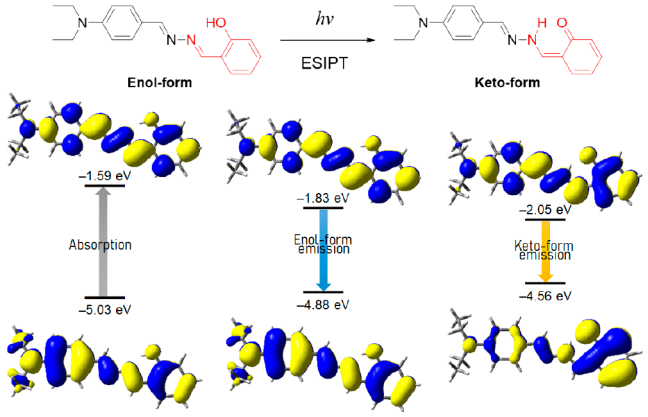

Figure 2. Molecular orbitals and energy levels of AP-DEA in the ground and excited states for enol and keto forms calculated with TD-DFT at the level of B3LYP/6-31G* based on solvation of THF.

1.76 Å for O−H and N···H, respectively). Simultaneously, the energy levels of LUMO of keto-form were lower than that of enol-form (−2.05 and −1.83 eV, respectively, for enol- and keto-forms of AP-DEA), indicating that enol−keto tautomerization in the excited state is thermodynamically favored for AP-based AIEgens (Figure 2). Besides, in terms of the ratio of oscillator strength of keto-form to that of enol-form (Table S2), AP-DEA had the most keto-emission than the other, which agreed with the experimental result.

Single Crystal Analysis. To further gain insight into AIE features of as-prepared AIEgens, their single-crystals were carefully analyzed (Figures 3, S8−S10, and Table S6). The torsion angles of the whole conjugated skeleton were so small, implying that AP-based AIEgens had coplanar conformation as well as suitable intramolecular H-bonding distance (1.89−1.91 Å for N···H−O) and angle (141.66−146.82° for N−H−O) to be helpful for ESIPT-active property. The packing of molecules was cross arrangement (Figures 3, S9, and S10), which reduced the intermolecular π−π overlap, avoiding the energy loss of excited molecules nonradiatively. The molecular packing was mainly constructed by the multiple intermolecular interaction such as CH···O (2.44−2.66 Å) and CH···π (2.76−2.88 Å). These collective interactions could not only restrict the molecular rotations to decline nonradiative pathway to bring about solid-luminescence, but also rigidify and planarize the molecular conformation to facilitate the ESIPT of phenolic hydrogen from oxygen to nitrogen.

Colocalization Imaging. The ESIPT-active AIEgens having both the hydrophilic azonomethylphenol (AP) moiety and the hydrophobic alkyl-amino-phenyl segment inspires us to serve them as the LDs-targeting probe in biological imaging. HeLa cells were incubated with AIEgens for 30 min and

DOI: 10.1021/acs.analchem.8b04736
Anal. Chem. 2019, 91, 2169−2176

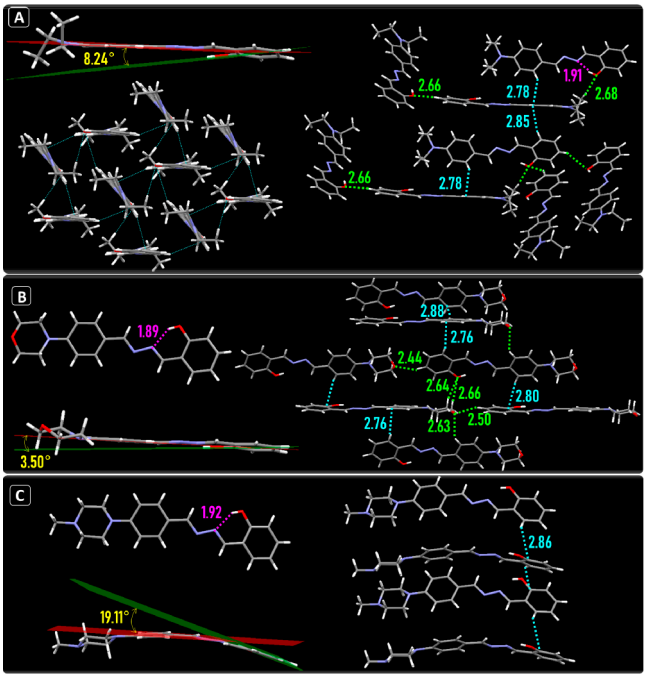

Figure 3. XRD crystallographic structures and their intermolecular interactions of (A) AP-DEA, (B) AP-ML, and (C) AP-PZ, in which the unit of bond length is Å.

observed by using confocal laser scanning microscopy (Figures 4–6).

However, we found that only AP-DEA showed the best specific targeting to LDs after colocalization with commercially available LDs probe, Nile red (Figure 4). According to the previous report,[41,42] the molecular properties of neutral LDs probes could be explained by two factors: (i) amphiphilicity

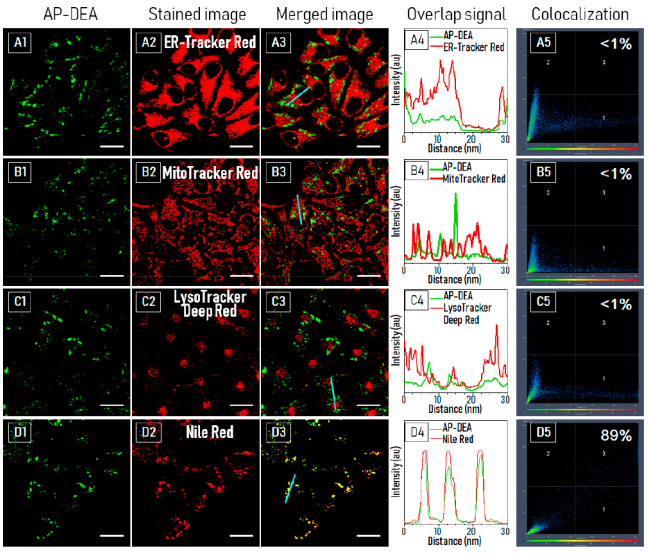

Figure 4. Colocalization images of HeLa cells costained with AP-DEA and ER-Tracker Red (A1–A3), MitoTracker Red (B1–B3), LysoTracker Deep Red (C1–C3), and Nile red (D1–D3). Excitation wavelength: 405 nm for AP-DEA and 560 nm for commercial probes (1% laser power). Concentrations: 1 μM for AP-DEA and 500 nM for commercial probes. Scale bar = 20 μm. (A4–D4) Overlap fluorescence signal of drew light-blue line of (A3–D3). (A5–D5) Colocalization images and Pearson correlation coefficient.

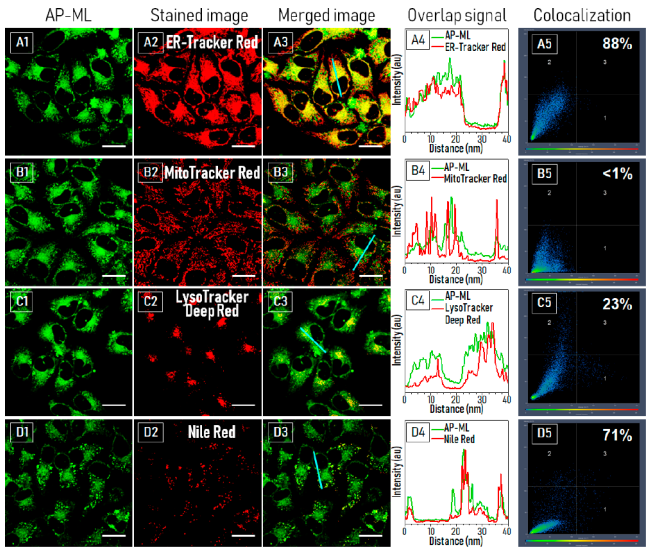

Figure 5. Co-localization images of HeLa cells costained with AP-ML and ER-Tracker Red (A1–A3), MitoTracker Red (B1–B3), LysoTracker Deep Red (C1–C3) and Nile red (D1–D3). Excitation wavelength: 405 nm for AP-ML and 560 nm for commercial probes (1% laser power). Concentrations: 1 μM for AP-ML and 500 nM for commercial probes. Scale bar = 20 μm. (A4–D4) Overlap fluoresce signal of drew light-blue line of (A3–D3). (A5–D5) Co-localization images and Pearson correlation coefficient.

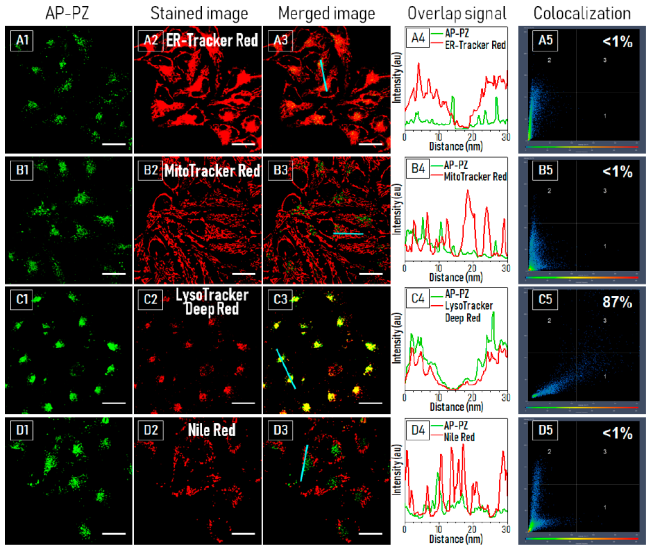

Figure 6. Colocalization of HeLa cells costained with AP-PZ and ER-Tracker Red (A1–A3), MitoTracker Red (B1–B3), LysoTracker Deep Red (C1–C3), and Nile red (D1–D3). Excitation wavelength: 405 nm for AP-PZ and 560 nm for commercial probes (1% laser power). Concentrations: 1 μM for AP-PZ and 500 nM for commercial probes. Scale bar = 20 μm. (A4–D4) Overlap fluoresce signal of drew light-blue line of (A3–D3). (A5–D5) Colocalization images and Pearson correlation coefficient.

index (AI), the lipophilicity domain of amphiphilic molecule, <3.50;[42] (ii) pharmaceutical chemists' parameter, logarithm of octanol–water partition coefficient (Log *P*),[43] that is, overall ratio of lipophilicity (as positive values) to hydrophilicity (as negative values) of molecule, >5.00.[41,44] AI values of all AIEgens were less than the standard value, 3.5, where the AP segment was as hydrophilic segment (Scheme S2). The Log *P* values of AP-DEA, AP-ML, and AP-PZ estimated with

DOI: 10.1021/acs.analchem.8b04736
Anal. Chem. 2019, 91, 2169–2176

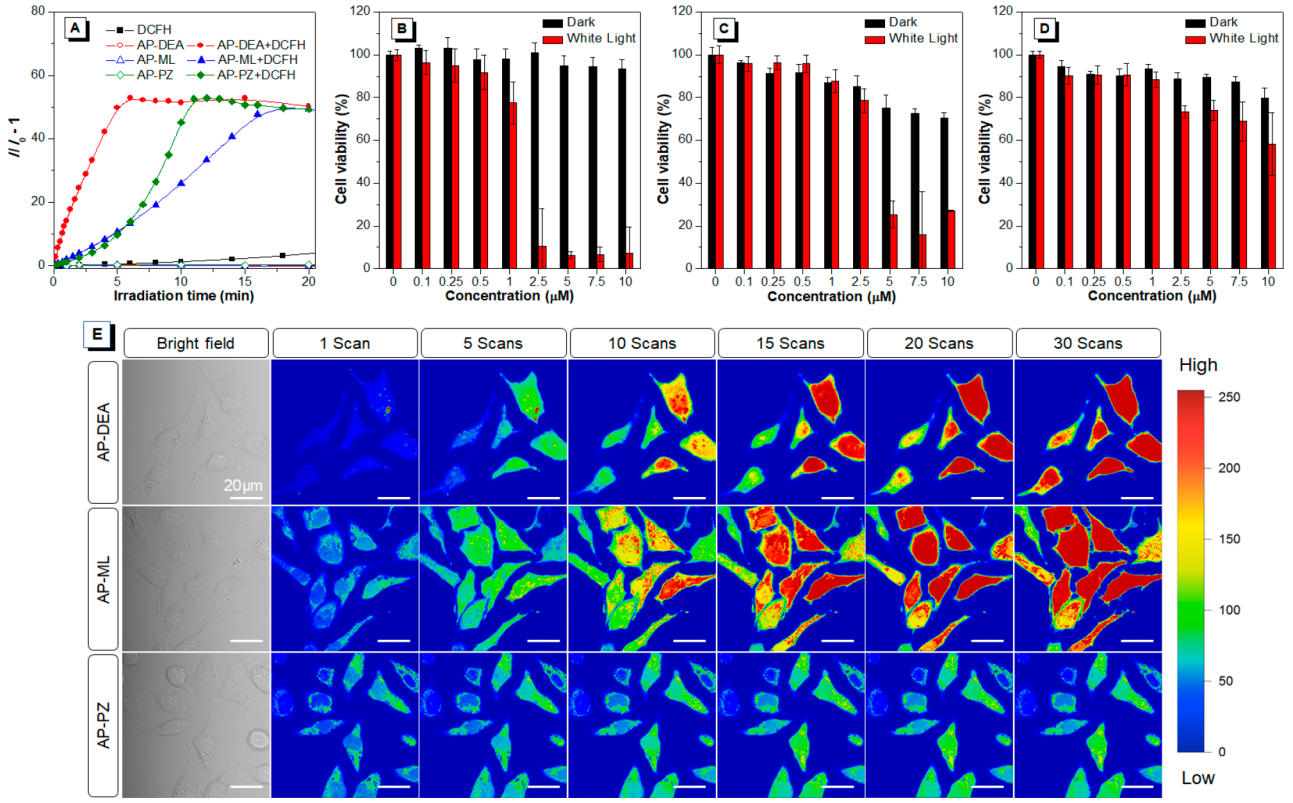

Figure 7. (A) Relative change in fluorescence intensity ($I/I_0 - 1$) at 525 nm of DCFH, AP-based AIEgens (AP-DEA, AP-ML and AP-PZ), mixtures of DCFH and AP-based AIEgens in PBS upon white light irradiation for different times. Concentrations: 10 μM for AP-based AIEgens and 1 μM for DCFH. (B–D) Cytotoxicity of HeLa cells stained with different concentrations of (B) AP-DEA, (C) AP-ML, and (D) AP-PZ, determined by MTT assay in dark and under white light irradiation for 30 min, respectively. Light power: 10 mW cm^{-2}. (E) Time- and strength-dependent confocal laser scanning microscopy (CLSM) images of HeLa cells after incubation with AP-based AIEgens (10 μM) and DCFH-DA (40 μM) via the different scanning times. Excitation wavelength: 488 nm for DCF fluorogen. Emission wavelength: 490–600 nm for DCF fluorogen. Scanning rate: 22.4 s for per scan. Scale bar: 20 μm.

ChemBioDraw software were 5.00, 3.92, and 4.08, respectively, which were higher for the hydrophilic starting material (H-AP, 1.13). The main reason why only AP-DEA could specifically target to LDs might be that its molecular structure had good proportion of lipophilic to hydrophilic segments. Thus, we could observe that AP-DEA (green color) had high colocalization with the commercial LDs probe, Nile red (Figure 4).

AP-ML and AP-PZ incorporate lysosome-targeting moieties, morpholine and piperazine, that motivate us to observe their colocalization of biological imaging with the commercial lysosome-targeting probe, LysoTracker Deep Red (Figures 5 and 6). It was found that lysosomes were only lit up specifically by AP-PZ. According to the staining process into lysosomes, once lipophilic AP-PZ diffuse into lysosomes, the acidic environment will protonate the piperazine groups and the positively charged AP-PZ accumulate inside the lysosome trapped by their inability to cross the membrane. Thus, we reasonably speculated that more basic piperazine moiety of AP-PZ was favorable to target the acidic organelle, lysosomes (pH 4.50).[3]

Surprisingly, AP-ML located and accumulated in ER largely rather than lysosome with moderate specificity (Figure 5). Combining molecular properties of the most of ER probes, one kind could be specified as 6 > AI > 3.5, 6 > log P > 0, and structural charge >0.[41] Moreover, the general ER probes such as ER-Tracker Red (Scheme S1) had an inner-salt structure, favoring for targeting to ER organelle.[7] By contrast, AP-ML was a rare neutral ER probe. Though AP-ML also stained some organelles such as LDs and lysosome, the relatively high colocalization with ER could be observed clearly (Figure 5A3–D3). Besides, compared with the commercial probe, AP-ML with a facile synthesis, mass production, low cost, and high Pearson correlation coefficient (88%) will be more popular with the industry.

It is worth mentioning that the position and specificity of organelle-targeting for AP-based probes would be adjusted simply from LDs, ER to lysosome through the modification of functional groups (diethylamino, morpholine or 1-methyl-piperazine) in the phenyl ring. This design strategy via ESIPT-active moiety (H-AP) to construct AIE probes fast and efficiently will inspire us for more research conceptions, like the functional Swiss knife. Moreover, photostability is a key parameter for evaluating the fluorescent probes. As shown in Figure S11, AP-DEA showed the best photostability than the heterocyclic alkyl-substituent constructed probes, AP-ML and AP-PZ, contributed from the best AIE performance of the former.

ROS Analysis and Imaging. The efficient and continuous ROS generation is a critical step for photodynamic therapy (PDT),[45] and thus the ability of ROS generation for AP-based AIEgens upon white light irradiation was evaluated. According to the analysis of ROS generation efficiency (Figures 7A and S12), in the presence of AP-based AIEgens, the emission

DOI: 10.1021/acs.analchem.8b04736
Anal. Chem. 2019, 91, 2169–2176

intensity of DCFH,[46] served as an indicator and exhibited the "turn-on" fluorescent signal activated by ROS, gradually enhanced about 50-fold with the increase of irradiation time by white light, whereas that of AP-based AIEgens or DCFH alone were dim or very weak. The maximum of the relative emission intensity $(I/I_0 - 1)$ showed little difference after irradiated for 20 min due to that the similar concentration of DCFH indicator was used. Additionally, AP-DEA displayed remarkably fast and effective growth of ROS generation in comparison with AP-ML and AP-PZ.

To clarify the relationship between ROS effect and cellular growth, their cytotoxicity of AP-DEA, AP-ML, and AP-PZ was further evaluated by the method of 3-(4,5-dimethyl-2-thiazolyl)-2,5-diphenyltetrazolium bromide (MTT) assay in the presence of white light irradiation for 30 min (Figure 7B–D),[21,47] whereas that in the dark was the control. Although MTT assay in the dark had some experimental errors from the cellular stress effect and interference of probes taken up by cells,[48] the overall results showed no obvious inhibitory phenomenon in the growth of HeLa cells, even in culture medium with high concentration (10 μM) except for AP-ML. Accordingly, under a general LED white light irradiation, the distinct cytotoxicity of AIEgens was observed, indicating they could generate ROS in the complexity of biological system. The effect of intracellular ROS generation for AP-DEA was far superior to the other two, in which 10% cell viability was detected in the presence of low concentration of AP-DEA (2.5 μM) and light irradiation, which conforms the ROS generation efficiency (Figure 7A). The AP-based AIEgens accumulating in specific organelle and producing ROS upon light irradiation were further observed in vitro (Figures 7E and S13). A dim or very weak fluorescent signal was detected after one scan, but gradually increasing DCF fluorescence could be observed upon the addition of scanning times. After 15 scans (about 6 min), the fluorescent signals of AP-DEA and AP-ML were very strong, suggesting that both probes could generate ROS better in the complexity of biological system in comparison with AP-PZ, which was coincident with the above MTT results under white light irradiation. Through the structural modification on the phenyl ring of benzaldehyde derivatives, the tunable targeting organelles and ROS-generation for ESIPT-active AIEgens would have more competitive advantage in comparison with the commercial small-molecule probes, which have been usually low photostability, complex modification, and high interference from background fluorescence resulting from their small Stokes shift. In addition, to further investigate with two-photon fluorescence imaging upon excitation wavelength of 780 nm (Figures S14 and S15), bright fluorescent signals and PDT effects could be preliminarily observed as well, implying that ESIPT-active AIEgens were promising two-photon probes for in vivo organelle-targeting and photodynamic ablation of cancer cells.[45]

CONCLUSIONS

The ESIPT-active AIEgens with organelle-targeting functions and ROS generation ability, AP-DEA, AP-ML, and AP-PZ, were successfully designed and synthesized by a facile, high-yielding, and one-step condensation reaction. Through the organelle-targeting regulating strategy, the location of probe-targeting and generating rate of ROS could be adjusted simultaneously. Furthermore, the proposed ESIPT-active H-AP unit will be full of inspiration to design the new organelle-targeting AIE probes, such as mitochondria or cell membrane tackers, and new generation of functional probes by modifying the active hydroxyl-group of AIEgens into responsive sensors in the future.

ASSOCIATED CONTENT

Supporting Information

The Supporting Information is available free of charge on the ACS Publications website at DOI: 10.1021/acs.analchem.8b04736.

Photophysical measurements, fluorescence decay curves, theoretical calculation data, XRD crystallographic analyses, and time-dependent CLSM images (PDF).

.cif file of $C_{18}H_{21}N_3O$, chemical formula weight 295.38 (CIF).

.cif file of $C_{18}H_{18}N_3O_2$, chemical formula weight 308.35 (CIF).

.cif file of $C_{19}H_{22}N_4O$, chemical formula weight 322.40 (CIF).

AUTHOR INFORMATION

Corresponding Author

*E-mail: tangbenz@ust.hk.

ORCID

Jen-Shyang Ni: 0000-0002-6727-2401
Zhen-Qiang Yu: 0000-0002-0862-9415
Ryan T. K. Kwok: 0000-0002-6866-3877
Ben Zhong Tang: 0000-0002-0293-964X

Author Contributions

†These authors contributed equally.

Notes

The authors declare no competing financial interest.

ACKNOWLEDGMENTS

We are grateful for financial support from the National Science Foundation of China (21788102, 21490570, 21490574, and 81501591), Science and Technology Plan of Shenzhen (JCYJ20170307173739739 and JCYJ20160229205601482), the Research Grants of Council of Hong Kong (16301614, 16305015, N_HKUST604/14, A-HKUST605/16, C2014-15G, and C6009-17G), the Innovation of Technology Commission (ITC-CNERC14SC01 and ITS/254/17), and China Postdoctoral Science Foundation (2016M602538 and 2018T110896). We also acknowledge the technical support received from AIEgen Biotech Co., Ltd.

REFERENCES

(1) Walther, T. C.; Farese, R. V., Jr. *Annu. Rev. Biochem.* **2012**, *81*, 687–714.
(2) Beller, M.; Thiel, K.; Thul, P. J.; Jackle, H. *FEBS Lett.* **2010**, *584*, 2176–2182.
(3) Xue, F.; Wei, P.; Ge, X.; Zhong, Y.; Cao, C.; Yu, D.; Yi, T. *Dyes Pigm.* **2018**, *156*, 285–290.
(4) Zhang, X.; Wang, K.; Liu, M.; Zhang, X.; Tao, L.; Chen, Y.; Wei, Y. *Nanoscale* **2015**, *7*, 11486–11508.
(5) Han, T.; Deng, H.; Qiu, Z.; Zhao, Z.; Zhang, H.; Zou, H.; Leung, N. L. C.; Shan, G.; Elsegood, M. R. J.; Lam, J. W. Y.; Tang, B. Z. *J. Am. Chem. Soc.* **2018**, *140*, 5588–5598.
(6) Yuan, Y.; Liu, B. *Chem. Sci.* **2017**, *8*, 2537–2546.
(7) Xiao, H.; Wu, C.; Li, P.; Gao, W.; Zhang, W.; Zhang, W.; Tong, L.; Tang, B. *Chem. Sci.* **2017**, *8*, 7025–7030.

DOI: 10.1021/acs.analchem.8b04736
Anal. Chem. 2019, 91, 2169–2176

(8) Ermakova, Y. G.; Sen, T.; Bogdanova, Y. A.; Smirnov, A. Y.; Baleeva, N. S.; Krylov, A. I.; Baranov, M. S. *J. Phys. Chem. Lett.* **2018**, *9*, 1958−1963.
(9) Verwilst, P.; Kim, H. R.; Seo, J.; Sohn, N. W.; Cha, S. Y.; Kim, Y.; Maeng, S.; Shin, J. W.; Kwak, J. H.; Kang, C.; Kim, J. S. *J. Am. Chem. Soc.* **2017**, *139*, 13393−13403.
(10) Azria, D.; Blanquer, S.; Verdier, J.-M.; Belamie, E. *J. Mater. Chem. B* **2017**, *5*, 7216−7237.
(11) Wang, Y.; An, R.; Luo, Z.; Ye, D. *Chem. - Eur. J.* **2018**, *24*, 5707−5722.
(12) Zhang, P.; Nie, X.; Gao, M.; Zeng, F.; Qin, A.; Wu, S.; Tang, B. Z. *Mater. Chem. Front.* **2017**, *1*, 838−845.
(13) Xu, S.; Zhang, X.; Liu, P. *Biochim. Biophys. Acta, Mol. Basis Dis.* **2018**, *1864*, 1968−1983.
(14) Wang, D.; Su, H.; Kwok, R. T. K.; Hu, X.; Zou, H.; Luo, Q.; Lee, M. M. S.; Xu, W.; Lam, J. W. Y.; Tang, B. Z. *Chem. Sci.* **2018**, *9*, 3685−3693.
(15) Gu, X.; Kwok, R. T. K.; Lam, J. W. Y.; Tang, B. Z. *Biomaterials* **2017**, *146*, 115−135.
(16) Poynton, F. E.; Bright, S. A.; Blasco, S.; Williams, D. C.; Kelly, J. M.; Gunnlaugsson, T. *Chem. Soc. Rev.* **2017**, *46*, 7706−7756.
(17) Feng, X.; Li, Y.; He, X.; Liu, H.; Zhao, Z.; Kwok, R. T. K.; Elsegood, M. R. J.; Lam, J. W. Y.; Tang, B. Z. *Adv. Funct. Mater.* **2018**, *28*, 1802833.
(18) Chen, W.; Gao, C.; Liu, X.; Liu, F.; Wang, F.; Tang, L. J.; Jiang, J. H. *Anal. Chem.* **2018**, *90*, 8736−8741.
(19) Zhang, P.; Zhao, Z.; Li, C.; Su, H.; Wu, Y.; Kwok, R. T. K.; Lam, J. W. Y.; Gong, P.; Cai, L.; Tang, B. Z. *Anal. Chem.* **2018**, *90*, 1063−1067.
(20) Wang, Y.-L.; Fan, C.; Xin, B.; Zhang, J.-P.; Luo, T.; Chen, Z.-Q.; Zhou, Q.-Y.; Yu, Q.; Li, X.-N.; Huang, Z.-L.; Li, C.; Zhu, M.-Q.; Tang, B. Z. *Mater. Chem. Front.* **2018**, *2*, 1554−1562.
(21) Zheng, Y.; Lu, H.; Jiang, Z.; Guan, Y.; Zou, J.; Wang, X.; Cheng, R.; Gao, H. *J. Mater. Chem. B* **2017**, *5*, 6277−6281.
(22) Chen, Y.; Zhang, W.; Zhao, Z.; Cai, Y.; Gong, J.; Kwok, R. T. K.; Lam, J. W. Y.; Sung, H. H. Y.; Williams, I. D.; Tang, B. Z. *Angew. Chem., Int. Ed.* **2018**, *57*, 5011−5015.
(23) Hu, F.; Yuan, Y.; Wu, W.; Mao, D.; Liu, B. *Anal. Chem.* **2018**, *90*, 6718−6724.
(24) Mei, J.; Leung, N. L. C.; Kwok, R. T. K.; Lam, J. W. Y.; Tang, B. Z. *Chem. Rev.* **2015**, *115*, 11718−11940.
(25) Ni, J.-S.; Zhang, P.; Jiang, T.; Chen, Y.; Su, H.; Wang, D.; Yu, Z.-Q.; Kwok, R. T. K.; Zhao, Z.; Lam, J. W. Y.; Tang, B. Z. *Adv. Mater.* **2018**, *30*, 1805220.
(26) Qin, W.; Zhang, P.; Li, H.; Lam, J. W. Y.; Cai, Y.; Kwok, R. T. K.; Qian, J.; Zheng, W.; Tang, B. Z. *Chem. Sci.* **2018**, *9*, 2705−2710.
(27) Xie, X.; Tang, F.; Liu, G.; Li, Y.; Su, X.; Jiao, X.; Wang, X.; Tang, B. *Anal. Chem.* **2018**, *90*, 11629−11635.
(28) Ning, J.; Tian, Z.; Wang, B.; Ge, G.; An, Y.; Hou, J.; Wang, C.; Zhao, X.; Li, Y.; Tian, X.; Yu, Z.; Huo, X.; Sun, C.; Feng, L.; Cui, J.; Ma, X. *Mater. Chem. Front.* **2018**, *2*, 2013−2020.
(29) Ni, J.-S.; Liu, H.; Liu, J.; Jiang, M.; Zhao, Z.; Chen, Y.; Kwok, R. T. K.; Lam, J. W. Y.; Peng, Q.; Tang, B. Z. *Mater. Chem. Front.* **2018**, *2*, 1498−1507.
(30) Butler, T.; Wang, F.; Sabat, M.; Fraser, C. L. *Mater. Chem. Front.* **2017**, *1*, 1804−1817.
(31) Kaewmati, P.; Yakiyama, Y.; Ohtsu, H.; Kawano, M.; Haesuwannakij, S.; Higashibayashi, S.; Sakurai, H. *Mater. Chem. Front.* **2018**, *2*, 514−519.
(32) Zhang, X.; Shi, J.; Shen, G.; Gou, F.; Cheng, J.; Zhou, X.; Xiang, H. *Mater. Chem. Front.* **2017**, *1*, 1041−1050.
(33) Wu, K.; Zhang, T.; Wang, Z.; Wang, L.; Zhan, L.; Gong, S.; Zhong, C.; Lu, Z. H.; Zhang, S.; Yang, C. *J. Am. Chem. Soc.* **2018**, *140*, 8877−8886.
(34) Keshav, K.; Kumawat, M. K.; Srivastava, R.; Ravikanth, M. *Mater. Chem. Front.* **2017**, *1*, 1207−1216.
(35) He, T.; Niu, N.; Chen, Z.; Li, S.; Liu, S.; Li, J. *Adv. Funct. Mater.* **2018**, *28*, 1706196.
(36) Wang, Z.; Zhou, F.; Wang, J.; Zhao, Z.; Qin, A.; Yu, Z.; Tang, B. Z. *Sci. China: Chem.* **2018**, *61*, 76−87.
(37) Tian, M.; Sun, J.; Tang, Y.; Dong, B.; Lin, W. *Anal. Chem.* **2018**, *90*, 998−1005.
(38) Wang, Z.; Gui, C.; Zhao, E.; Wang, J.; Li, X.; Qin, A.; Zhao, Z.; Yu, Z.; Tang, B. Z. *ACS Appl. Mater. Interfaces* **2016**, *8*, 10193−101200.
(39) Kim, S.-H.; Gwon, S.-Y.; Burkinshaw, S. M.; Son, Y.-A. *Dyes Pigm.* **2010**, *87*, 268−271.
(40) Thiyagarajan, S. K.; Suresh, R.; Ramanan, V.; Ramamurthy, P. *Chem. Sci.* **2018**, *9*, 910−921.
(41) Horobin, R. W.; Rashid-Doubell, F.; Pediani, J. D.; Milligan, G. *Biotech. Histochem.* **2013**, *88*, 440−460.
(42) Horobin, R. W.; Rashid-Doubell, F. *Biotech. Histochem.* **2013**, *88*, 461−476.
(43) Ishikawa, M.; Hashimoto, Y. *J. Med. Chem.* **2011**, *54*, 1539−1554.
(44) Niu, G.; Zhang, R.; Kwong, J. P. C.; Lam, J. W. Y.; Chen, C.; Wang, J.; Chen, Y.; Feng, X.; Kwok, R. T. K.; Sung, H. H. Y.; Williams, I. D.; Elsegood, M. R. J.; Qu, J.; Ma, C.; Wong, K. S.; Yu, X.; Tang, B. Z. *Chem. Mater.* **2018**, *30*, 4778−4787.
(45) Alifu, N.; Dong, X.; Li, D.; Sun, X.; Zebibula, A.; Zhang, D.; Zhang, G.; Qian, J. *Mater. Chem. Front.* **2017**, *1*, 1746−1753.
(46) Bourré, L.; Thibaut, S.; Briffaud, A.; Rousset, N.; Eléouet, S.; Lajat, Y.; Patrice, T. *J. Photochem. Photobiol., B* **2002**, *67*, 23−31.
(47) Wu, W.; Mao, D.; Hu, F.; Xu, S.; Chen, C.; Zhang, C. J.; Cheng, X.; Yuan, Y.; Ding, D.; Kong, D.; Liu, B. *Adv. Mater.* **2017**, *29*, 1700548.
(48) Zhang, X.; Zhang, X.; Wang, S.; Liu, M.; Tao, L.; Wei, Y. *Nanoscale* **2013**, *5*, 147−150.

DOI: 10.1021/acs.analchem.8b04736
Anal. Chem. 2019, 91, 2169−2176